Midlatitude ionospheric *D* region: height, sharpness and solar zenith angle

Neil R. Thomson[1], Mark A. Clilverd[2], and Craig J. Rodger[1]

[1]Physics Department, University of Otago, Dunedin, New Zealand

[2]British Antarctic Survey, Cambridge, UK

Key Points:

- Ionospheric lower *D* region electron density height profiles measured mid-summer at a mid- to high geomagnetic dip latitude of 52.5 degrees
- Midday *D* region height and sharpness measured as 72.8 +-0.2 km and 0.345 +-0.015 per km defining the electron density height profile
- New technique has higher accuracy and higher latitude giving improved baseline for *D* region radio propagation and particle precipitation

Abstract

VLF radio amplitude and phase measurements are used to find the height and sharpness of the *D* region of the ionosphere at a mid- to high geomagnetic dip latitude of ~52.5°. The two paths used are both from the 23.4 kHz transmitter, DHO, in north Germany with the first path being northwards and mainly over the sea along the west coast of Denmark over a range of ~320-425 km, and the second, also mainly all-sea, to a single fixed recording receiver at Eskdalemuir in Scotland (~750 km). From plots of the measured amplitudes and phases versus distance for the first of these paths compared with calculations using the US Navy code, ModeFinder, the Wait height and sharpness parameters of the *D* region at midday in summer 2015 are found to be H' = 72.8 ±0.2 km and $ß$ = 0.345 ±0.015 km^{-1} at a solar zenith angle ~33°. From phase and amplitude measurements at other times of day on the second path, the daytime changes in H' and $ß$ as functions of solar zenith angle are determined from shortly after dawn to shortly before dusk. Comparisons are also made between the modal ModeFinder calculations and wave hop calculations, with both giving similar results. The parameters found here should be useful in understanding energy inputs to the *D* region from the radiation belts, solar flares or transient luminous events. The midday values may be sufficiently precise to be useful for monitoring climate change.

1 Introduction

The lowest edge of the Earth's ionosphere, typically found at heights around 70 km by day and around 85 km by night, forms the upper boundary, or ceiling, of the Earth-ionosphere waveguide for VLF radio waves (at least for 3-30 kHz) and so determines many of the properties of this waveguide which is bounded below by the Earth's surface (often sea water).

VLF signals from man-made transmitters and from natural sources, such as lightning, propagate in this waveguide with fairly low attenuation and are thus detectable and often measurable after travelling distances of 12-15 Mm or more. The man-made VLF signals are often used for communicating with submerged military submarines because, not only do they have ranges of many thousands of kilometres horizontally, but their low frequencies also enable these signals to penetrate many metres into seawater. Man-made VLF signals are also used by scientific networks such as AARDDVARK (Antarctic-Arctic Radiation-belt Dynamic Deposition VLF Atmospheric Research Konsortia) in order to determine energy inputs into the upper atmosphere from energetic particle precipitation [*Clilverd et al.*, 2009; http://www.physics.otago.ac.nz/space/AARDDVARK_homepage.htm]. Detailed knowledge of the undisturbed characteristics of the *D* region are important in identifying space weather perturbations of radio signals, and in being able to calculate the fluxes of particles involved [*Neal et al.*, 2015]. The VLF radio signals propagating from distant lightning are used by networks such as WWLLN (World-Wide Lightning Location Network) to find the locations of the lightning strikes and hence thunderstorms etc. [*Dowden et al.*, 2008]. Also commonly propagating in the Earth-ionosphere waveguide are signals from or via the magnetosphere such as whistlers, whistler-mode signals, hiss, chorus and other VLF emissions. *Silber and Price* [2017] have recently reviewed the use of narrowband VLF to study the *D* region and the many space physics phenomena it is sensitive to, including anthropogenic climate change.

By day, lower *D* region ionization is generated mainly by Lyman-α from the Sun ionizing neutral NO molecules at altitudes mainly above ~70 km, and by galactic cosmic rays ionizing all the neutral constituents, and normally dominating at altitudes below ~70 km [e.g., *Banks and Kockarts*, 1973]. As the solar zenith angle increases, the unidirectional Lyman-α from the Sun has less ionizing effect, both towards dawn or dusk, and towards higher latitudes. In contrast the omni-directional galactic cosmic rays do their ionizing equally at all times of day. However, they are more intense nearer the poles than near the equator due to the greater shielding effect of the more horizontal Earth's magnetic field near the equator [e.g. *Størmer,* 1955]. This means that daytime *D* region electron number densities vary depending on latitude and time of day. Thus in equatorial regions near midday, Lyman-α is very dominant, strongly ionizing (NO) down to ~70km below which the Lyman-α is rapidly absorbed by the neutral atmospheric O_2. This relatively 'sharp' lower boundary characterizes the equatorial lower *D* region, in particular resulting in lower attenuation at VLF (because of the narrower height region for electron-neutral collisions). In contrast, away from midday or at higher latitudes, the solar zenith angle is higher resulting in lower penetration of Lyman-α, but the galactic cosmic ray intensity is the same, or higher at higher latitudes, thus producing the same or more electron density at altitudes below

~70 km. This results in the *D* region electron density height profile tending to be less sharp and more attenuating than for equatorial noon.

By using short-path, nearly all-sea, VLF propagation, *Thomson* [2010] and *Thomson et al.* [2012, 2014] have determined Wait height and sharpness parameters [*Wait and Spies*, 1964] in the ranges *H'* = 69.3-70.5 km and β = 0.47-0.49 km^{-1} at low latitudes at midday. On a mid-latitude short path from NAA, Cutler, Maine to Prince Edward Island, also at midday, *Thomson et al.* [2011a] found *H'* = 71.8 km and β = 0.335 km^{-1}. Although more than half of this path was over the sea with good well-known conductivity, most of the rest was over rather low conducting ground, resulting in significant uncertainty. These widely-used *Wait and Spies* [1964] height, *H'*, and sharpness, β, parameters approximate the electron number density, *N* (m^{-3}), as a function of height, *z*, using the equation

$$N(z) = 1.43 \times 10^{13} \exp(-0.15H') \exp[(\beta - 0.15)(z - H')].$$

All of the above short path measurements involved making a set of amplitude and phase measurements near (~100 km from) the transmitter, where the ground wave dominates, to effectively determine the amplitude (radiated power) and phase of the transmitter, and then making a second set of measurements ~300 km from the transmitter where the subionospherically reflected signal forms a significant modal minimum with the ground wave, giving good ionospheric sensitivity. Measurements at intermediate locations were not generally practicable due to factors such as the presence of sea, lack of ready access via roads or low, uncertain, rapidly varying, ground conductivity.

Here we measure the amplitude and phase of signals from the 23.4 kHz transmitter (DHO) near the north coast of Germany northwards over a nearly all-sea path at multiple locations along the west coast of Jutland, Denmark, over a range of ~320-425 km. Consistent, meaningful measurements were possible and practicable due to a convenient road up the west coast, and the uniform and high conductivity of the ground. These measurements are then compared with calculated results for this path from US Navy code ModeFinder [*Morfitt and Shellman*, 1976] over a range of possible *D* region ('Wait') height and sharpness parameters, *H'* and β. The best match between the measurements and calculations enabled the appropriate values of *H'* and β for the ionospheric *D* region to be determined at this latitude. This was particularly so for midday; for other times of day, between dawn and dusk, use is also made of diurnal recordings, also in July 2015, of the amplitude and phase of 23.4 kHz from DHO at Eskdalemuir in Scotland, a ~750-km nearly all-sea-path with a very similar latitude range. These two propagation paths used are shown in Figure 1.

The determination of these higher latitude *D* region parameters fills a gap in the characterization of the *D* region needed for techniques which use VLF propagation such as WWLLN and AARDVARK, discussed above, to monitor lightning and magnetospheric energetic particle precipitation. These observed parameters and their resulting electron densities should also be useful for testing *D* region modeling at these high mid-latitudes. The improved accuracy in *D* region height from the new multi-position technique here may also be useful in monitoring global warming changes.

2 Portable Loop VLF Phase and Amplitude Measurements

All the amplitude and phase measurements of DHO signals made in Denmark (along the west coast of Jutland) were made with a custom-designed portable loop consisting of about 80 turns of copper wire firmly mounted in a fixed rectangular wooden frame ~50 cm x 60 cm equipped with suitable electronics to measure amplitude and phase delay, with respect to a GPS 1-s pulse, of a selected VLF frequency. The stability and hence reproducibility in amplitude and phase was ~0.1-0.3 dB and ~0.1-0.3 μs depending on measurement conditions. The absolute accuracy of the amplitude measurements was probably ~±0.5 dB, in good conditions, but the method used here requires only relative (reproducible) accuracy at the various measurement sites used in West Jutland.

Potential measurement sites were normally selected to be at least a few tens of metres from the main north-south coastal road (the '181') and from wire fences, and also preferably more than 100 m or so from obvious power (electricity) lines etc. Before being selected, each site was tested to check that consistent amplitude and phase measurements were obtained for at least a few tens of metres around the site. A selected site also needed to give consistent readings compared with nearby sites (say 0.2-5 km away). Along the west coast of Jutland, with its rural low population density and good conducting sandy soils near the sea, it proved to be fairly straightforward to find suitable sites.

DHO, like many other VLF transmitters, in particular like most US Navy transmitters, is modulated with 200 baud MSK. DHO's nominal frequency is 23.4 kHz so that means that during any 5-ms bit period it radiates either 23.35 kHz or 23.45 kHz. A set of measurements, normally taken within 3-4 minutes at each site, consisted firstly of orienting the portable loop to maximum amplitude on 23.35 kHz and then recording both amplitude, in dB >1 μV/m, and phase delay, in μs. This was then repeated at 23.35 kHz for the other directional maximum, i.e., with the loop rotated through 180°. These two steps were then repeated at 23.45 kHz, giving 4 phase readings and 4 amplitude readings which were then averaged to give a single phase reading and a single amplitude reading. Such measurements were made on 13 days, 5-17 July 2015. For phase, the portable loop measurements in μs were converted into degrees for comparison with the US Navy modelling code, ModeFinder, which outputs phase in degrees. For example, at the site near the intersection of the main north-south road (the '181') and Damgårdvej, 360 km (~north) from the DHO transmitter, the averaged measured phase at 1240 UT (near midday) on 5 July 2015 was 18.025 μs while at 1157 UT (also near midday) on 8 July 2015 it was 21.15 μs (details available in the supporting information), an apparent increase in phase delay of 21.15 - 18.025 = 3.125 μs which is equivalent to a phase change of -360 x 3.125 μs x 23400 Hz = -26.3 degrees. This rather large change in apparent phase over these 3 days is due mainly to the transmitter having (1) a small frequency offset from its nominal 23.4 kHz and (2) occasional phase jumps. Fortunately these can both be rather accurately corrected for as discussed in the next two sections, enabling phase measurements on separate days and separate locations to be compared, and so used to measure the height and sharpness of the ionospheric *D* region along the path over the North Sea to the west coast of Jutland.

3 Monitoring the DHO Transmitter and Correcting for its Phase and Amplitude Changes

While the portable loop phase and amplitude measurements were being made at locations on the DHO-Denmark path in July 2015, the phase and amplitude of DHO were also being monitored continuously by a fixed recorder at St. John's, Newfoundland, Canada. Both this recorder and that at Eskdalemuir (section 6, below) are GPS-referenced "UltraMSK" receivers [http://ultramsk.com] and are part of the AARDDVARK network. The 4.2 Mm path from DHO across the Atlantic to St. John's, is very stable near midday particularly in summer and so serves as a useful monitor for the DHO transmitter's amplitude and phase stability as shown in Figure 2. (The period 07-08 UT on each day is shown as blank because the transmitter is then off-air for maintenance.) As can be seen, the amplitude of DHO on 13 July was clearly about 1.5 dB below the amplitudes on the other observation days and so the amplitudes measured with the portable loop on the DHO-Denmark path were able to be adjusted accordingly for that day. As can also be seen, particularly in the amplitude plot, there was significant solar flare activity on 6 July 2015 and so portable loop measurements made on that day were excluded from the DHO-Denmark path analysis since the aim was to measure normal quiet conditions.

The DHO transmitter, though nominally on 23.4 kHz, has a significant long term frequency offset which causes its phase to advance by just over one cycle (360º) in 4.5 hours. To make the phase of DHO easier to interpret, the recording frequency at St. John's is set to 23400.00006173 Hz, or equivalently above 23.4 kHz by exactly one cycle per 4.5 hours which is also exactly 80º per hour and exactly an integer number (16) of cycles (360º) in 3 days (used in the next section). Inspection of the phase panels in Figure 2 shows the actual frequency of DHO is slightly higher than the recording frequency by about 29º/day or 1.2º/hour. This can be seen partly from the (small) positive slopes of the phase lines, but mainly from the typical phase changes from midday to midday. In assessing the day-to-day changes in phase, account needs to be taken of possible random phase jumps, particularly during the off-air hour from 07-08 UT each day (fewer in the second period, 11-17 July, than in the first, 5-11 July). Also, the phases in this type of recorder are nearly always modulo 90º because the recorder is averaging the phases of the two sidebands (nominally 23.35 kHz and 23.45 kHz) of the MSK modulation and the phase of each of the sidebands in MSK is always modulo 180º [e.g. *Thomson*, 1981].

4 Comparing Observed and Calculated Phases and Amplitudes to Find Midday *H'* and *ß*

Figure 3 shows the (58) amplitudes and (58) phases of DHO near midday, from the portable loop measurements along the west coast of Jutland, Denmark, as functions of distance from DHO as individual points on the (12) specified days. At some sites on some days, 2 or sometimes 3 sets of portable loop measurements were able to be made near midday. In these cases the 2 or 3 results at each site on the particular day were averaged and plotted as just one point in each of the two panels in Figure 3; hence, in each of the two plots, there is no more than one point per site per day. The lines in Figure 3 show the ModeFinder-calculated phases and amplitudes for the specified ionospheric *D* region values of *H'* (height in km) and *ß* (sharpness in km^{-1}).

The ModeFinder amplitudes are for a radiated power of 300 kW. In order for the measured amplitudes to match these calculated amplitudes all the (portable loop) measured amplitudes were increased by 5.0 dB except that those on 13 July 2015 were increased by an extra 1.5 dB (as discussed above). These adjustments are thus compensating for the transmitter radiating less than 300 kW during the measurement period here of 5-17 July 2015. For the phases, the portable loop measurements (in µs relative to GPS 1-s pulses) needed to be adjusted for the transmitter phase changes (drifts and jumps) by using the recorded phases in Figure 2 as outlined below.

Phase measurements are normally relative, as here, so some reference baseline needs to be chosen. In the phase panel in Figure 3 it can be seen that the measured phase at 360 km from DHO (near midday) on 5 July is shown as 33.9º (the choice of this value is discussed below). The placement of the other phase values relative to this one is now illustrated. As discussed at the end of Section 2, the portable loop measured an apparent phase change of 3.125 µs ≡ -26.3º at the 360-km site between 1240 UT on 5 July and 1157 UT on 8 July (3 days less 43 minutes). But the DHO transmitter phase changed during this time and so this -26.3º needs to be adjusted for these changes. Figure 2 shows that the DHO phase (as measured by the recorder at St. John's) changed over 3 days from -90º at 13 UT on 5 July to 125º at 13 UT on 8 July which is an increase of 125º - (-90º) = 215º ≡ 35º (modulo 90º). As mentioned in the previous section, 3 days is an integer multiple (16) of the difference period between (exactly) 23.4 kHz and the recorder frequency (23400.00006173 Hz) so that this 35º (modulo 90º) is also the phase change over 3 days at (exactly) 23.4 kHz. But the interval between the portable loop measurements is less than 3 days by 43 minutes. In this 43 minutes the phase of DHO (relative to GPS) would have advanced by (80º + 1.2º) per hour (Section 3) i.e. by 43/60 x (80+1.2) = 57.3º + 0.9º. So the corrected change is -26.3 – 35 + 57.3 + 0.9 = -3.1º from the 33.9º on 5 July giving the 30.8º shown for 8 July at 360 km. All the other phases at 360 km in Figure 3 were determined in the same way.

For the phases measured at the sites with ranges other than 360 km from DHO, the measured phases (in µs relative to GPS 1-s) were adjusted by allowing for the free-space speed of light, 0.29979 km/µs. For this purpose the distances of the sites from DHO were determined using the Vincenty algorithm [*Vincenty*, 1975] from the latitudes and longitudes measured with a portable GPS receiver on site at the times of measurements and later checked with Google Earth. The center of the DHO transmitter was estimated from Google Earth as 53.07925 N, 7.61416 E but it is the relative distances of the portable loop measurement sites from DHO rather than their absolute distances which are important; so the center of DHO is not needed to great accuracy.

For the ModeFinder calculations in Figure 3, the geomagnetic dip, azimuth and magnitude for July 2015 at an altitude ~72 km were used: 69º, 4º (E. of N.), and 48 µT. Typically the first 20 modes were summed (though the first ~15 modes would usually have sufficed) to get B_y (the magnetic field parallel to the ground and perpendicular to the propagation direction) since this is what the (vertical) portable loop measures, but the magnitude measurements were recorded in µV/m (using $E_B = cB_y$ where c is the speed of light) as has been the convenient custom for VLF measurements. As explained above, the measured amplitudes were adjusted (upwards on the graph) by 5.0 dB to match the ModeFinder-calculated amplitudes (6.5 dB for

13 July only). Similarly for the phases, because the reference phase level for the measurements was arbitrary, the measured phases were also shifted (all by the same amount, vertically on the graph) until they gave the best match to the ModeFinder-calculated phases. In particular, this resulted in the 33.9º at 360 km on 5 July 2015 used above. This was the end result of a somewhat iterative process because the appropriate values of *H'* and *ß* were initially not known and so had to be adjusted to get the best matches in distance and shape between the measured and calculated amplitudes and phases.

From the amplitude plots in the lower panel of Figure 3, it can be seen that the best fit is close to *H'* = 72.8 km and *ß* = 0.35 km^{-1}. The method of estimating the likely error made use of the other ModeFinder-calculated lines shown in the plot. In particular, if *H'* were lowered or raised by 0.3 km (i.e. *H'* = 72.5 km with *ß* = 0.35 km^{-1} or *H'* = 73.1 km with *ß* = 0.35 km^{-1}), the calculated line would clearly be rather too far to the left or too far to the right respectively of the measured points, implying the likely error in *H'* is somewhat less than ± 0.3 km. If *ß* alone were decreased or increased, the minimum would be less or more deep respectively but the curves would also move a little to the left or right respectively. To make a change in *ß* of ± 0.2 km^{-1} easier to visualize, in particular in terms of the depth of the minimum, *H'* was also changed to keep the minimum at the same range from the transmitter (~358 km) resulting in *H'* = 72.5 km with *ß* = 0.37 km^{-1} and *H'* = 73.1 km with *ß* = 0.33 km^{-1} being plotted for comparisons. From these last two plots it can be seen that the error in *ß* is likely to be slightly less than ± 0.2 km^{-1}. The phase plots in the upper panel of Figure 3 give the same best fit value of *H'* = 72.8 km as the amplitude plots but a slightly lower value of *ß* = 0.34 km^{-1}. A somewhat similar procedure for error, as used for the amplitude plots above, was applied to the phase plots resulting in a similar or very slightly larger error for the phase plots alone as compared with the amplitude plots.

Combining the results from both the amplitude and phase plots in Figure 3 thus gives an overall best match for *H'* = 72.8 ±0.2 km and *ß* = 0.345 ±0.015 km^{-1} for the midday summer ionospheric *D* region over the North Sea at a geomagnetic dip latitude of 52.5° and a solar zenith angle of ~33º (i.e. the sun ~33º from the vertical).

5 Uniqueness of the *H'* and *ß* and comparison with a Wave Hop Code

There is always a possible concern that, although the ModeFinder-calculated amplitudes and phases using *H'* = 72.8 km and *ß* = 0.345 km^{-1} match the measured amplitudes and phases very well, they may not be the only values of *H'* and *ß* that fit the measurements. The upper two panels of Figure 4 show ModeFinder-calculated values of phase and amplitude for the same DHO-Denmark path (using $E_B = cB_y$ as in section 4) but using a much wider range of *H'* and *ß*. From these it can be clearly seen that there are no other likely values of *H'* and *ß* which could produce phases or amplitudes which would be similar to those from *H'* = 72.8 km and *ß* = 0.345 km^{-1}.

The US Navy code, ModeFinder, and its derivative, LWPC [*Ferguson and Snyder*, 1990], treat the space between the Earth's surface and the ionospheric *D* region as a waveguide and determine the properties of the modes which can propagate and then sum over the modes to get the amplitudes and phases at each location along the path. LWPC is designed to conveniently automatically segment (typically long) paths where the waveguide properties change significantly along the length of the path. It is otherwise very similar to ModeFinder but cannot output B_y needed here (as discussed in Section 4 and below) and does not seem to be quite as robust – e.g., away from midday at frequencies higher than those used here. ModeFinder is the most widely used and tested code; its stability over a wide range of conditions is very good. An alternative strategy is to treat the propagation as a number of waves or rays which reflect, once or up to many times, from the upper and lower edges of the waveguide in a series of hops and then these waves or rays are summed at the receiver. The Wave Hop code of *Berry and Herman* [1971] is probably the best known of these. As with Modefinder and LWPC, the Wave Hop code uses spherical rather than planar geometry, and also uses an anisotropic ionosphere for the reflection coefficients. For the short (320-425 km) path here, only up to two hops (and the ground wave) are actually needed. Only the 1-hop (single hop, single reflection) wave is comparable in magnitude with the ground wave at these short ranges. The 2-hop contribution is only ~3% of the total field (and so, although small at ~0.3 dB, is just marginally needed) while the 3-hop contribution <~0.2% (<~0.02 dB) and so is quite negligible. All of these codes (ModeFinder, LWPC and Wave Hop) calculate E_z (i.e. the vertical electric field) at the receiver. For the code versions available for this study, only ModeFinder could also calculate B_y (the horizontal magnetic field of the wave perpendicular to the propagation direction, which the portable loop measures). Thus comparisons between the three calculation codes needed to be made using E_z.

The lower two panels of Figure 4 show such comparisons (for a radiated power of 300 kW as in Figure 3). For ModeFinder and LWPC the best fit values of *H'* and *ß* from Figure 3 are used. For ModeFinder the values plotted are exactly those output by the code (‘MFz’ is for E_z and ‘MFy’ is for $E_B = cB_y$ as discussed above). For LWPC, the magnitudes of E_z output have been reduced by 0.22 dB because the modal excitation factors for LWPC are ~0.22 dB higher than for ModeFinder. The reason for this is not known but is not important here because it does not affect our comparison of (relative) amplitudes at different ranges (320-425 km); it would affect only the relationship between our amplitudes and the radiated power which is not important here. Also for LWPC, the phases output have been reduced by 90º because LWPC phases at each range are calculated relative to E_z directly beside the antenna while ModeFinder phases are relative to the antenna current. It can be seen that any difference between E_z from LWPC and E_z from ModeFinder is clearly negligible. The difference between these E_z and the $E_B = cB_y$ arises because $E_z = 2E_\perp \cos\theta$, where $E_\perp$ is the electric field perpendicular to the ray in the vertical plane of propagation in each of the down-going and reflected rays at angles θ to the horizontal, while $B_y = 2B_\perp$ (without the $\cos\theta$ factor) because the two $B_\perp$ are both horizontal as well as being perpendicular to their rays.

For the comparisons with Wave Hop in Figure 4, values of H' and $ß$ were chosen for Wave Hop to best match the phases and amplitudes from the H' and $ß$ used in ModeFinder in the best fits to the observed data in Figure 3. Thus if the E_z for H' = 72.8 km and $ß$ = 0.35 km^{-1} (amplitude) and H' = 72.8 km and $ß$ = 0.34 km^{-1} (phase) from ModeFinder in Figure 4 are thought of as representing the observed data, then it can be seen that the best fits from Wave Hop calculations would be H' = 72.8 km and $ß$ = 0.34 km^{-1} for amplitude and H' = 73.0 km and $ß$ = 0.32 km^{-1} for phase. This assumes that the differences between E_z and $E_B = cB_y$ for ModeFinder are very similar to what the differences between E_z and $E_B = cB_y$ would be for Wave Hop which seems quite likely. Thus if Wave Hop had been used alone, and Wave Hop had been able to calculate B_y (and so $E_B = cB_y$), the best average values for the path would likely have been H' = 72.9 km and $ß$ = 0.33 km^{-1} rather than the preferred best values from ModeFinder derived above: H' = 72.8 ±0.2 km and $ß$ = 0.345 ±0.015 km^{-1}.

In order to compare and match the Wave Hop and ModeFinder results in Figure 4, the Wave Hop phase results were all increased by 45º and the Wave Hop amplitude results were all reduced by 0.43 dB as indicated by the data labels in the lower two panels. The reasons for needing these adjustments are not precisely known but are presumably related to the excitation factors in ModeFinder (and LWPC). These differences in absolute phase and absolute amplitude are not important here because it is the measured variations with distance of the relative phases and amplitudes that are used in Figure 3 and the recorded variations with time of the relative phases and amplitudes that are used in section 6 below.

All of the above calculations have assumed an all-sea path. This is likely appropriate here but none-the-less ~70 km of the ~360 km path is over land at the transmitter end and over a very much smaller amount of land at the receiver end. ModeFinder (and Wave Hop) do not allow for paths which are partly over sea and partly over land. However, LWPC has a built-in ground conductivity map (for VLF) and has some capability to do this by segmenting the path, including performing mode-conversion at (abrupt) conductivity boundaries (though only for E_z). For most of North Germany (including the appropriate parts here) and for all of Jutland, LWPC's map gives the ground conductivity as 0.01 S/m which is relatively good being the same as most of the best conducting ground around the world - only a very small part of the world's land has a higher conductivity. In contrast, the conductivity for sea water is ~4 S/m while for poor conducting land it is ~0.001 – 0.0001 S/m.

The LWPC all-sea output, as in Figure 4, was compared with the output with 70 km of 0.01 S/m land at the transmitter end, with nothing else changed. The greatest change in amplitude (in the range 320-425 km) was an increase of just under 0.2 dB (at the minimum ~358 km) while the position of the minimum moved ~0.8 km towards the transmitter. From Figure 3 it can thus be estimated that, if this 70 km of 0.01 S/m land were taken into account, *H'* and β would be higher by ~0.06 km and ~0.005 km^{-1} respectively which are ~1/3 of the estimated errors in *H'* and β in section 4 (±0.2 km and ±0.015 km^{-1}). In reality the appropriate land conductivity is probably higher than 0.01 S/m because of its proximity to the sea resulting in seepage and sea spray. Also the conductivity values in LWPC are averages for roughly 100 km square blocks with the result that extreme closeness to the coast has not been fully taken into account. At the other end of the path, in Jutland, the receiving sites were all very close to the coast (<~5 km with many < 1 km). The coastal ground is very sandy and so porous to seawater; also the strong prevailing westerlies will be blowing salt spray across it. Hence, overall, it seems very likely that treating the path as all-sea is the most appropriate.

6 Variation of *H'* and *ß* with Solar Zenith Angle (SZA)

The techniques of sections 2- 4 above, used to find *H'* and *ß* at midday, could also be used to find *H'* and *ß* at other times of day (i.e., at higher solar zenith angles). This, however, involves some significant disadvantages. Near midday the SZA (the angle between the Sun and the zenith) and the ionosphere change very little over a period of 1-2 hours allowing measurements at many ranges during this time. However, at other times the SZA and the ionosphere change much faster with time making it much more difficult to achieve a series of measurements with a single portable loop system at different ranges along the path without measuring over several weeks to get averages of at least a few days over a range of times at each measurement site. This tends to be compounded by the ionospheric *D* region being less stable away from midday and so requiring more measurements and averaging.

Hence it is often more convenient to use a continuous, fixed recorder, if available, for measuring changes with SZA. The disadvantage with fixed recorders is that, although usually very stable, they are not usually well calibrated (quite often due to terrain issues) either in absolute phase or absolute amplitude. However, if suitable, calibrated, portable loop measurements have been made, as presented here in sections 2-4, then these can provide the calibrations for the fixed recorder.

While no fixed recordings for DHO to anywhere in Denmark were available, good phase and amplitude recordings for the same July 2015 period were available for the 748-km path DHO to Eskdalemuir, Scotland shown in Figure 1. As can be seen the latitude range for DHO-Eskdalemuir is very similar to that for the DHO-Jutland paths so that the *H'* and *ß* at midday for DHO-Jutland already determined here can be used to calculate (using ModeFinder) the midday amplitude and phase at Eskdalemuir, thus calibrating the Eskdalemuir recorder in amplitude and phase. The DHO-Eskdalemuir path, in contrast with the 4.2-Mm DHO-St. John's path, has the advantage of being quite short (748 km) so that the SZA varies very little along the path resulting in the SZA at the mid-point being very representative for the path.

The top two panels of Figure 5 show the experimentally observed variations with time for the phase and amplitude of DHO at Eskdalemuir averaged over many days around the times the portable loop measurements were made in Jutland in July 2015. Although not of great consequence, the averaging period for the amplitudes (16 days: 4-19 July) was longer than for the phases (8 days: 9-16 July). This was partly because the amplitudes tended to be a bit more variable and partly because they are very easily averaged. Three amplitude averages are plotted, for 4-11 July, for 12-19 July and for the whole period, 4-19 July, to indicate that a sufficient number of days have been averaged. Phase averaging requires more care to check that the small number of phase jumps (mainly at the transmitter) are dealt with appropriately. The 8-day period 9-16 July was chosen because it appeared to have very few phase jumps which were all readily corrected for, and the resulting phase plot (top panel, Figure 5) was adequately smooth. During this averaging process, the phase was fully corrected for the transmitter phase drifts (including the ~29º/day) as determined in section 3 using the St. John’s recorder.

The ModeFinder code with the values H' = 72.8 km and $ß$ = 0.345 km^{-1} from the midday Jutland North Sea portable loop measurements, was now used to compute the midday phase and amplitude for DHO at Eskdalemuir resulting in 120º and 68.8 dB. This then served as the calibration of the recorder at Eskdalemuir – i.e., the 48.7º at midday in the top panel of Figure 5 observed at Eskdalemuir is equivalent to the 120º from ModeFinder. Thus any of the (observed) phases in the top panel can be converted to ModeFinder degrees by adding 120º - 48.7º = 71.3º. Similarly, any of the (observed) amplitudes at Eskdalemuir in the 2nd top panel of Figure 5 can be converted to ModeFinder dB by adding 68.8 – (-54.7) = 123.5 dB. The bottom two panels of Figure 5 show the phase and amplitude results from ModeFinder calculations for the DHO-Eskdalemuir path (coloured points and lines) for the various values of *H'* and *ß* shown. The open black circles in all four panels show the observed values of phase and amplitude at Eskdalemuir (top two panels of Figure 5) converted to ModeFinder degrees and dB (bottom two panels of Figure 5) for comparison with the ModeFinder calculations which thus determines the values of *H'* and *ß* at the times shown. Although just 13 black circles are shown in each panel, twice as many observed values of phase and amplitude from the top two panels were used to find corresponding values of *H'* and *ß* in the bottom two panels; only half are actually shown to avoid any overlapping.

In the top two panels of Figure 6, the values of *H'* and *ß* found from the bottom two panels of Figure 5 are plotted as functions of UT. The mid-point of the DHO-Eskdalemuir path is at 54.32º N and 2.35º E and so, after allowing for 'the equation of time' on ~11 July 2015, the Sun is at its highest above the horizon (lowest SZA) at this (DHO-Eskdalemuir) mid-point at 1156 UT. Thus it can be seen from these two UT plots in Figure 6 that the *D* region peaks, in *H'*, and troughs, in *ß*, several minutes after local midday (i.e., several minutes after 1156 UT). This slight delay in the *D* region has been noticed before [e.g., *Thomson*, 1993]; it may be due to afternoon NO concentrations being larger than those in the morning [*Marsh and Russell*, 2000]. The small glitch in the *H'* and *ß* values just after local midday is related to the best fit for amplitude in Figure 3 being for *H'* = 72.8 km and *ß* = 0.35 km^{-1} while the best fit for phase was for *H'* = 72.8 km and *ß* = 0.34 km^{-1} and so the average, *H'* = 72.8 km and *ß* = 0.345 km^{-1} does not quite fit for either. Clearly this rather small discrepancy is fairly inconsequential here.

In the bottom two panels of Figure 6, the values of *H'* and *ß* from the top two panels are plotted as functions of solar zenith angle (SZA). SZA's less than ~32º never occur on this path; hence there are no data points between ~±32º. Curiously the data points on either side of midday appear to fit quite closely to straight lines in these SZA plots. While the reason for this is not completely clear, it does allow tentative extrapolations, as shown, to overhead sun (SZA = 0) for the path at *H'* ≈ 70 km and *ß* ≈ 0.40 km^{-1}. Of course, this cannot be compared with real overhead-Sun observations for this path, because the Sun is never so high in the sky for this path. But it can be compared with near equatorial regions where *Thomson et al.* [2014] found *H'* = 69.3 ±0.3 km and *ß* = 0.49 ±0.02 km^{-1} for an SZA ~10º in 2012. The difference in these *H'* values is due at least in part to the higher sunspot number in 2012 but is also likely within the experimental error particularly that on the extrapolated *H'* ≈ 70 km. The higher value of *ß* actually observed at low latitude (in 2012) will be mainly due to the lower level of galactic cosmic rays there (due to the greater shielding by the nearly horizontal geomagnetic field) resulting in fewer electrons at the lowest altitudes (below ~65-70 km).

7 Discussion, Summary and Conclusions

7.1 Midday at Geomagnetic Dip Latitude ~52.5º (DHO, Germany - North Sea – Jutland, Denmark)

The summer midday *D* region parameters found here H' = 72.8 ±0.2 km and $ß$ = 0.345 ±0.015 km^{-1}, at geomagnetic dip latitude 52.5º and SZA ~33º, can be compared with the July 2010 results of *Thomson et al.* [2011a] at a very similar geomagnetic dip latitude but with SZA ~23º on a similarly short path from NAA, Cutler, Maine, to Prince Edward Island (PEI), H' = 71.8 ±0.6 km and $ß$ = 0.335 ±0.025 km^{-1}. The details are summarized in Table 1.

The following factors contribute to the H' difference between these two sets of results. From Figure 6, it can be estimated that the 10º higher SZA for the Jutland path increases H' by ~0.9 km compared with the PEI path. The MSIS atmospheric model [https://omniweb.gsfc.nasa.gov/cgi/vitmo/vitmo_model.cgi] was used to calculate the nitrogen number density, [N_2], (as a proxy for the total air density) at the heights near H' at the mid-points of the paths. The values of [N_2] at each H' are shown in Table 1. For the NAA-PEI path, at H' = 71.8 km, the N_2 number density, as can be seen in Table 1, was 1.245 x 10^{21} m^{-3}, while the MSIS calculation for the DHO-Denmark path showed this same number density occurred ~0.6 km higher (i.e., at a height of ~72.4 km). The Jutland measurements in 2015 had a (ISES/NOAA) smoothed sunspot number (SSN) ~40 compared with ~17 for PEI in 2010; *Thomson et al.,* [2012] found a decrease in H' of ~0.75 km when the SSN increased from 5 to 60 from which it can be estimated that the higher SSN in 2015 would make H' lower than in 2011 by ~0.3

km. The overall effect is that *H′* for the Jutland path in 2015 would be predicted to be 0.9 + 0.6 - 0.3 = 1.2 km higher which is fairly close to the 72.8 – 71.8 = 1.0 km actually observed, being within the error in *H′* of ±0.6 km for the PEI path alone.

Just two factors contribute to the *ß* difference between the two sets of results. From Figure 6, it can be estimated that the 10º higher SZA for the Jutland path causes *ß* to be lower there by ~0.02 km^{-1} compared with the PEI path. The results of *Thomson et al.*, [2012] used above for *H'* are probably not appropriate for *ß* because the latitude was very low. However, *McRae and Thomson* [2000], at a mixture of mid- and low latitudes, observed a decrease in *ß* of ~0.05 (from 0.45 to 0.40) km^{-1} in going from an SSN of ~140 in 1991 to ~15 in 1995 from which an increase in *ß* of ~0.02 km^{-1} can be estimated from the SSN of 17 at PEI in 2010 rising to an SSN of ~40 at Jutland in 2015. Together these two changes cancel to essentially zero; this again compares reasonably well with the difference between the two observations: 0.335 ±0.025 km^{-1} for the PEI path in 2010 and *ß* = 0.345 ±0.015 km^{-1} here for the Jutland path in 2015.

7.2 The Effective Solar Zenith Angle near Midday for the DHO-Jutland Path

For the observation period here, centred on 11 July 2015, the SZA at the midpoint of the path, from DHO to the (modal) minimum near 360 km north of DHO, was 32.6° at midday (1134 UT). However, not all of the portable loop measurements could be made very close to midday because of the time required to travel between the measurement sites at the different distances from DHO, and the need to do the measurements over a period of <~ 2 weeks. Hence the effective average SZA during the Jutland measurements is slightly greater than 32.6° and needs to be estimated. In particular, although many of the measurements were made <~ 1 hour from midday, some, such as those at a range near 320 km, were made early, ~1000-1030 UT, when the SZA was ~36° and a few were made quite late, ~1300-1345 UT, when the SZA was ~36-41°. However, as discussed below, these early and late readings do not appear to significantly influence the choice of *H'* and β in Figure 3 for optimum fit. Specifically, the measurements at the greatest ranges 405 km and 423 km were made fairly close to midday.

The midpoint SZA is ≤33.5° between 1052 UT and 1215 UT, and ≤34.5° between 1033 UT and 1234 UT. Also, in the DHO-Eskdalemuir phase plot in Figure 5 it can be seen that the phase peak is centered 15-20 min after midday (i.e., 15-20 min after 1156 UT) so that the 1215 UT and 1234 UT can probably be extended to 1235 UT and 1254 UT respectively. From Figure 5 it can be seen that β changes by 0.40-0.29 =0.11 km^{-1} over an SZA change of ~60° or about 0.0018 km^{-1}/degree. Hence even 3° increase in effective average SZA (such as for 1000-1030 UT) results in much less than the midday error in β already allowed for here (±0.015 km^{-1}). Also in Figure 5, it can be seen that *H'* changes with SZA by about 0.09 km/degree and so a 1° uncertainty in SZA is nearly half the midday error of ±0.2 km already allowed for. However, an examination of Figure 3 shows that the measurements near 340-360 km are the most critical for determining *H'*, nearly all of which were taken in the time range 1100-1240 UT which means that the effective average SZA is probably nearer 33° than 34°.

7.3 Short Path Technique Comparisons

It is worthwhile to compare the short path VLF technique used here, with the short path VLF technique used previously on several occasions over the last few years to measure *H’* and *ß* particularly near (path) midday. Both techniques have measured both amplitude and phase with a calibrated portable loop. The previously used technique [*Thomson*, 2010; *Thomson et al.*, 2011a; *Thomson et al.*, 2012; *Thomson et al.*, 2014] typically measured the VLF amplitude at essentially just two distances from the transmitter – the first ~100 km from the transmitter where the ground wave dominates, to effectively get the amplitude and phase of the transmitter, and the second typically ~300 km from the transmitter, near the minimum between the ground wave and the ‘sky’ wave reflected from the ionosphere, to effectively measure the amplitude and phase after the reflection from the ionosphere and so determine the ionospheric height and sharpness (*H’* and *ß*). Normally several sets of measurements were made at sites within a few km of each of the two principal distances (~100 km and ~300 km) to assure that each of the sites were typical and free of interference. The two sites could be at or near small towns and the ~200 km of road between needed to be traversed only once or twice and did not need to be very direct and could have difficult geographic features. Quite often parks or other recreation areas in the (two) towns provided convenient measuring sites.

In contrast the technique used in this paper did not require going near (<~100 km) to the transmitter but made measurements at several distances along an approximate line from ~320 km to ~425 km from the transmitter. This resulted in an accuracy better by nearly a factor of two than typically achieved before. It does however, require some favourable factors. The road along the West Jutland coast of Denmark was lightly populated (low interference), lightly trafficked going fairly level, fairly straight and direct nearly radially from the transmitter thus enabling efficiency. The good uniform conductivity of the ground (sandy soil close to the sea-coast) was particularly important resulting in few anomalous readings due to ground conductivity issues (natural or man-made). Even better, most of the path from the transmitter was over the (highly and very uniformly conducting) sea as can be seen in Figure 1. An aeroplane (or possibly a boat) could, of course, potentially do even better but issues such as gain stability and interference would need to be carefully dealt with, and height would need to be recorded and used in the calculation comparisons.

7.4 Variation of *H'* and *ß* with Solar Zenith Angle

During daylight, *H'* increases and β decreases with increasing solar zenith angle [*Thomson*, 1993]. This is mainly due to the principal ionizing radiation, Lyman-α, penetrating the neutral atmosphere less deeply as the SZA increases but also, particularly for β, a very important contributing factor is that, for the lower part of the lower *D* region (below ~65-70 km), the dominant ionizing radiation comes from galactic cosmic rays which do not vary with SZA or time. Because the galactic cosmic ray intensity at ionospheric heights varies with geomagnetic shielding and hence geomagnetic latitude [e.g., *Heaps*, 1978], the variations with SZA in *H'* and β are dependent on geomagnetic latitude as has been observed and reported by *Thomson et al.* [2014]. The highest latitude path reported there was for NAU in Puerto Rico to St. John's in Canada for which the path mid-point is at a geographic latitude of 33º, and a geomagnetic dip latitude of 37º as compared with the much higher values of 54.5º and 52.5º respectively for the current path. From *Thomson et al.* [2014], when the mean SZA on the NAU to St. John's path changed from 33º to 70º, *H'* changed from 71.6 km to 76.9 km and β from 0.41 km^{-1} to 0.285 km^{-1}, while from Figure 6, for the DHO-Eskdalemuir path, for the same SZA change from 33º to 70º, *H'* changed from 72.8 km to 76.2 km and β from 0.345 km^{-1} to 0.275 km^{-1}. The lower β and the smaller changes in β and *H'* with SZA on the DHO-Eskdalemuir path are likely due to the greater proportion of non-SZA-dependent ionization (galactic cosmic rays) on this higher latitude path.

7.5 Summary and Conclusions

Amplitude and phase measurements of VLF radio signals measured, as functions of distance from the transmitter mainly over the sea, on good uniform conducting ground, preferably near the modal minimum, 300-400 km from the transmitter, can give very good results for the height and sharpness of the lowest edge of the Earth's ionosphere such as the specific result here of *H'* = 72.8 ±0.2 km and *ß* = 0.345 ±0.015 km^{-1} for DHO in north Germany across the North Sea to the west coast of Denmark at a mean geomagnetic dip latitude of ~52.5º in July of 2015 at an SZA of ~33º. Such measurements are also useful for calibrating fixed recorders which can then be conveniently used to extend these results to determine the changes in this lowest ionospheric (*D* region) edge with SZA at other times of day, as was done here. The accuracy of this type of measurement at midday, particularly any changes in the 'reference' height, *H'*, may have the potential over time to be a measure of the effects of global warming, including any associated cooling in the stratosphere/mesosphere [*Roble and Dickinson,*1989; *Taubenheim et al.,* 1997; *Akmaev et al.*, 2006; *Lastovicka*, 2008; *Peters et al*., 2017].

Acknowledgements

The phase meter used with the portable loop measurements was skilfully designed and constructed by David Hardisty. The recorded data used in Figures 2 and 5 can be found at http://psddb.nerc-bas.ac.uk The raw data measurements underlying Figure 3 are available in the supporting information. The solar zenith angles were found at https://www.esrl.noaa.gov/gmd/grad/solcalc/ and the geomagnetic dip angles at https://ngdc.noaa.gov/geomag-web/#igrfwmm. The sunspot numbers came from http://www.swpc.noaa.gov/products/solar-cycle-progression and ftp://ftp.swpc.noaa.gov/pub/weekly/RecentIndices.txt

References

Akmaev, R. A., V. I. Fomichev and X. Zhu (2006), Impact of middle- atmospheric composition changes on greenhouse cooling in the upper atmosphere, *J. Atmos. Sol. Terr. Phys., 68*, 1879–1889, doi:10.1016/j.jastp.2006.03.008.

Banks, P. M., and G. Kockarts (1973), *Aeronomy*, Academic, New York.

Berry, L.A. and J.E. Herman (1971), *A wave hop propagation program for an anisotropic ionosphere*, OT/ITS Research Rep. 11, U.S. Dept. of Commerce, Boulder, Colo.

Clilverd, M. A., C. J. Rodger, N. R. Thomson, J. B. Brundell, Th. Ulich, J. Lichtenberger, N. Cobbett, A. B. Collier, F. W. Menk, A. Seppälä, P. T. Verronen, and E. Turunen (2009), Remote sensing space weather events: the AARDDVARK network, *Space Weather*, 7, S04001, doi:10.1029/2008SW000412.

Dowden, R.L., R.H. Holzworth, C.J. Rodger et al. (2008), World-Wide Lightning Location Using VLF Propagation in the Earth-Ionosphere Waveguide, *IEEE Antennas and Propagation Magazine*, *50(5)*, 40-60.

Ferguson, J. A. and F. P. Snyder (1990), Computer programs for assessment of long wavelength radio communications, version 1.0: Full FORTRAN code user's guide, *Naval Ocean Systems Center Tech. Doc. 1773, DTIC AD-B144 839*, Def. Tech. Inf. Cent., Alexandria, Va.

Heaps, M.G. (1978), Parameterization of the cosmic ray ion-pair production rate above 18 km. *Planet. Space Sci.*, 26, 513-517.

Lastovicka, J., R. A. Akmaev, G. Beig, J. Bremer, J. T. Emmert, C. Jacobi, M. J. Jarvis, G. Nedoluha, Y. I. Portnyagin, and T. Ulich (2008), Emerging pattern of global change in the upper atmosphere and ionosphere, *Ann. Geophys.*, *26(5)*, 1255–1268, doi:10.5194/angeo-26- 1255-2008.

Marsh, D.R. and J.M. Russell (2000), A tidal explanation for the sunrise/sunset anomaly in HALOE low-latitude nitric oxide observations, *Geophys. Res. Lett.*, *27(19)*, 3197-3200.

McRae, W. M. and N. R. Thomson (2000), VLF phase and amplitude: daytime ionospheric parameters, *J. Atmos. Sol.-Terr. Phys.*, 62(7), 609-618.

Morfitt, D. G. and C. H. Shellman (1976), MODESRCH, an improved computer program for obtaining ELF/VLF/LF mode constants in an Earth-Ionosphere Waveguide. *Naval Electr. Lab. Cent. Interim Rep. 77T, NTIS Accession ADA032573*, Natl. Tech. Inf. Serv., Springfield, VA.

Neal, J.J., C. J. Rodger, M. A. Clilverd, N. R. Thomson, T. Raita, and T. Ulich (2015), Long-term determination of energetic electron precipitation into the atmosphere from AARDDVARK subionospheric VLF observations, *J. Geophys. Res. Space Physics*, *120*, 2194-2211, doi:10.1002/2014JA020689.

Peters, D.H.W., G. Entzian and P. Keckhut (2017), Mesospheric temperature trends derived from standard phase-height measurements, *J. Atmos. Sol.-Terr. Phys*., http://dx.doi.org/10.1016/j.jastp.2017.04.007

Roble, R. G. and R. E. Dickinson (1989), How will changes in carbon dioxide and methane modify the mean structure of the mesosphere and thermosphere?, *Geophys. Res. Lett.*, *16(12)*, 1441-1444.

Silber, I. and C. Price (2017), On the use of VLF narrowband measurements to study the lower ionosphere and the mesosphere–lower thermosphere, *Surv Geophys 38*, 407–441, doi:10.1007/s10712-016-9396-9.

Størmer, C. (1955), *The Polar Aurora*, Clarendon Press, Oxford.

Taubenheim, J., G. Entzian, and K. Berendorf (1997), Long-term decrease of mesospheric temperature, 1963-1995, inferred from radiowave reflection heights, *Adv. Space Res. 20(11)*, 2059–2063.

Thomson, N. R. (1981), Whistler mode signals: Spectrographic group delays, *J. Geophys. Res., 86(A6)*, 4795-4802.

Thomson, N. R. (1993), Experimental daytime VLF ionospheric parameters, *J. Atmos. Terr. Phys.*, *55*, 173-184.

Thomson, N.R. (2010), Daytime tropical D region parameters from short path VLF phase and amplitude, *J. Geophys. Res.*, *115*, A09313, doi:10.1029/2010JA015355.

Thomson, N.R., M. A. Clilverd and C. J. Rodger (2011a), Daytime midlatitude *D* region parameters at solar minimum from short-path VLF phase and amplitude, *J. Geophys. Res.*, *116*, A03310, doi:10.1029/2010JA016248.

Thomson, N.R., C. J. Rodger and M. A. Clilverd (2011b), Daytime *D* region parameters from long-path VLF phase and amplitude, *J. Geophys. Res.*, *116*, A11305, doi:10.1029/2011JA016910.

Thomson, N.R., C. J. Rodger and M. A. Clilverd (2012), Tropical daytime lower D-region dependence on sunspot number, *J. Geophys. Res.*, *117*, A10306, doi:10.1029/2012JA018077.

Thomson, N.R., M. A. Clilverd and C. J. Rodger (2014), Low-latitude ionospheric *D* region dependence on solar zenith angle, *J. Geophys. Res. Space Physics*, *119*, doi:10.1002/2014JA020299.

Vincenty, T. (1975), Direct and inverse solutions of geodesics on the ellipsoid with application of nested equations, *Survey Review*, *23(*176), 88-93.

Wait, J.R., and K.P. Spies (1964), Characteristics of the Earth-ionosphere waveguide for VLF radio waves. *NBS Tech. Note 300*, Natl. Bur. of Stand., Boulder, Colo.

Table 1. Comparison of paths at different latitudes. (SZA = Solar Zenith Angle, SSN = Smoothed Sunspot Number, [N_2-MSIS] = N_2 number density in units of 10^{21} m^{-3})

Path	**Geog. Lat.**	**Geog. Long.**	**Dates (inclusive)**	**SZA**	**SSN**	β **(km^{-1})**	***H'* (km)**	**[N_2]-MSIS**	
DHO(23.4kHz)-> Denmark	54.7°N	7.9° E	5-17 July 2015	33°	41	0.345	72.8	1.181	
NAA(24.0kHz)-> PEI	45.5°N	65.3° W	2-5 July 2010	23°	17	0.335	71.8	1.245	
NPM(21.4kHz)-> Hawaii	20.5°N	157.0° W	19-25 Aug 2012	10°	58	0.490	69.3	1.481	

Figure Captions

Figure 1. The two VLF radio paths over the North Sea from transmitter DHO (23.4 kHz) used to find the lower *D* region electron densities here.

Figure 2. Phases and amplitudes of DHO recorded at St. John's, Newfoundland, to monitor DHO while the principal measurements were being made with a portable loop along the west coast of Denmark.

Figure 3. Phases and amplitudes of DHO (23.4 kHz) measured near midday on the west coast of Denmark compared with ModeFinder calculations for various appropriate *D* region electron densities modeled with height, *H'*, and sharpness, β. (150705 = 5 July 2015 UT etc.; 72.8/0.35 indicates *H'*= 72.8 km and β = 0.35 km^{-1} etc.)

Figure 4. The top two panels compare ModeFinder calculations for *H'*= 72.8 km and β = 0.35 km^{-1} with those for a much wider range of *H'* and β than in Figure 3 (to check for uniqueness). The bottom two panels compare calculations for E_z from the Wave Hop code ('WH'), from LWPC ('LWz') and from ModeFinder for E_z ('MFz') and for the $E_B = cB_y$ ('MFy') used in the top two panels, and in Figure 3 for comparisons with the portable loop measurements. (See text for more details.)

Figure 5. The top two panels show the average phases and amplitudes of DHO as functions of time recorded ~748 km to the N.W. at Eskdalemuir, Scotland, July 2015. In the bottom two panels these phases and amplitudes are compared with ModeFinder calculations to determine the dependences of *H'* and β on time of day.

Figure 6. Ionospheric *D* region height, *H'*, and sharpness, β, as functions of time and solar zenith angle for geomagnetic dip latitude 52.5º found here from the VLF observations on the 748-km path, DHO to Eskdalemuir.

Path	**Geog. Lat.**	**Geog. Long.**	**Dates (inclusive**	**SZA**	**SSN**	**® (km^{-1})**	***H′* (km)**	**[N_2]-MSIS**
DHO(23.4 kHz) -> Denmark	54.7° N	7.9° E	5-17 July 2015	33°	41	0.345	72.8	1.181
NAA(24.0 kHz) -> PEI	45.5° N	65.3° W	2-5 July 2010	23°	17	0.335	71.8	1.245
NPM(21.4 kHz) -> Hawaii	20.5° N	157.0° W	19-25 Aug 2012	10°	58	0.490	69.3	1.481

Figure 1.

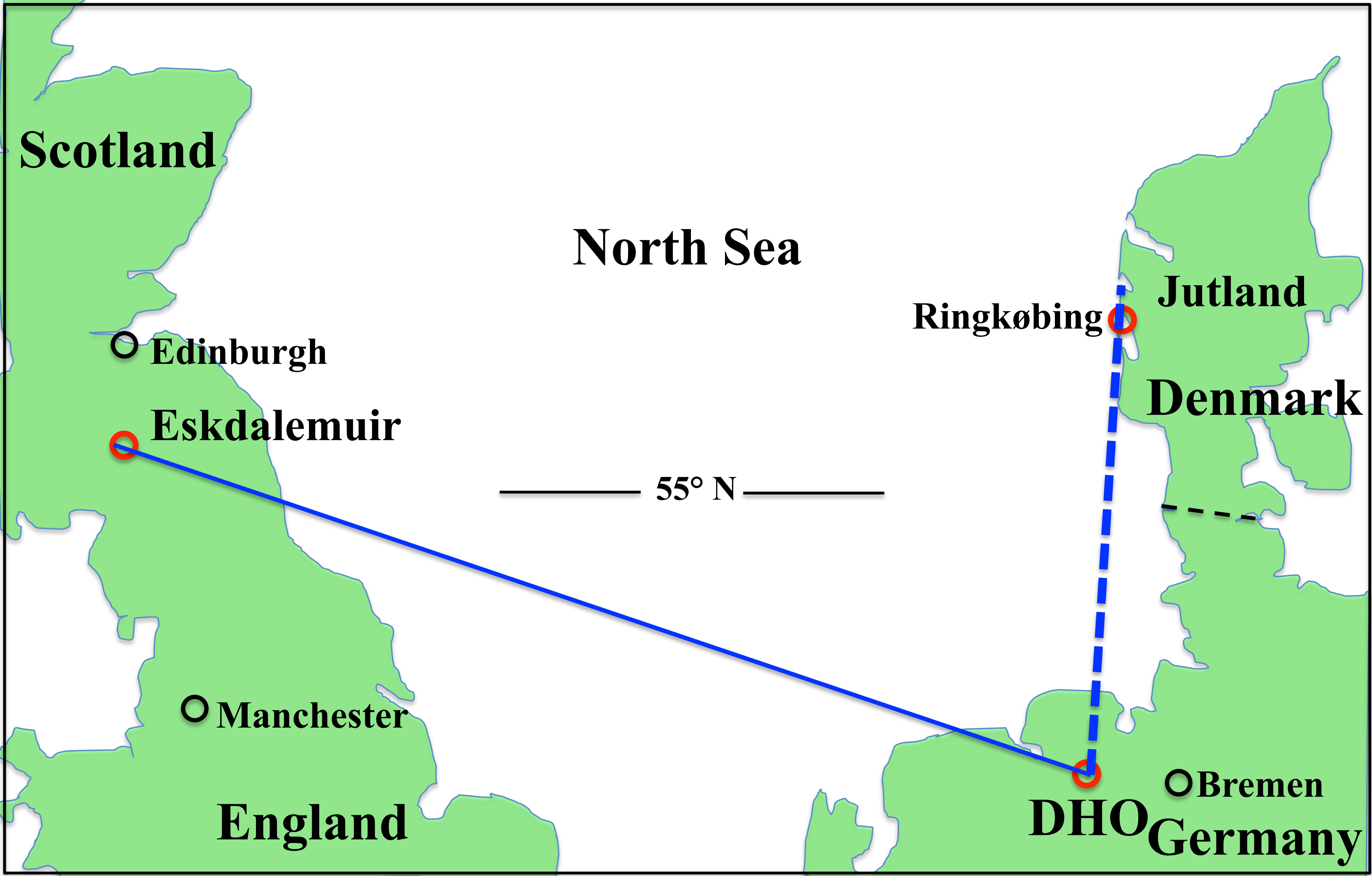

Scotland
North Sea
Jutland
Ringkøbing
Edinburgh
Denmark
Eskdalemuir
55° N
Manchester
Bremen
DHO
England
Germany

Figure 2.

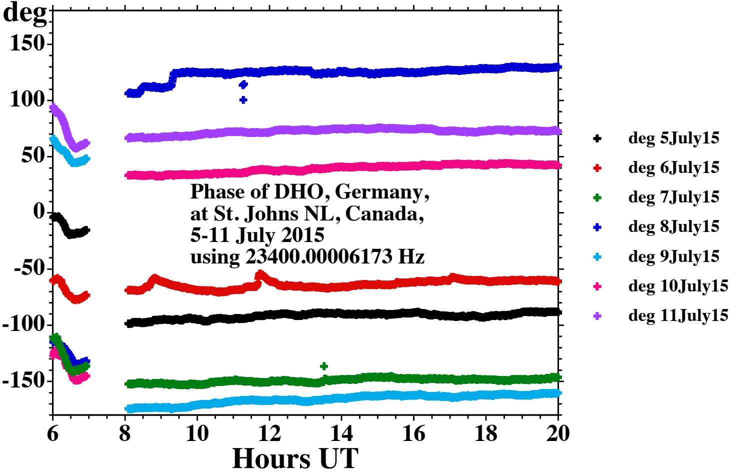
deg
150
100
50
0
-50
-100
-150
6
8
10
12
14
16
18
20
Hours UT
Phase of DHO, Germany,
at St. Johns NL, Canada,
5-11 July 2015
using 23400.00006173 Hz
deg 5July15
deg 6July15
deg 7July15
deg 8July15
deg 9July15
deg 10July15
deg 11July15

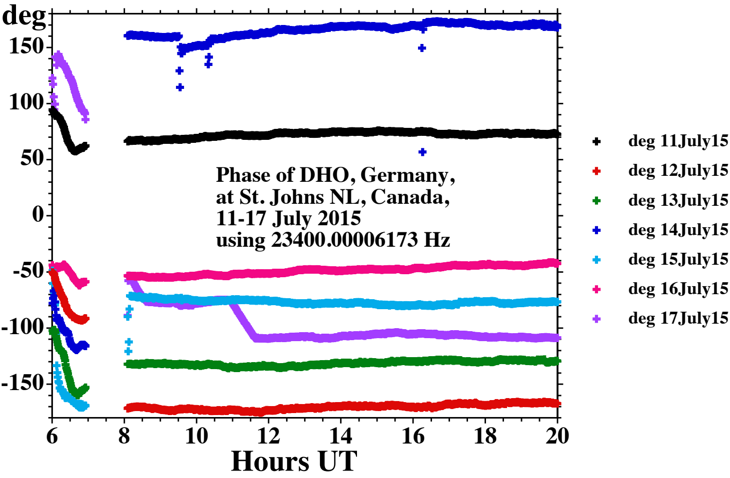
deg
150
100
50
0
-50
-100
-150
6
8
10
12
14
16
18
20
Hours UT
Phase of DHO, Germany,
at St. Johns NL, Canada,
11-17 July 2015
using 23400.00006173 Hz
deg 11July15
deg 12July15
deg 13July15
deg 14July15
deg 15July15
deg 16July15
deg 17July15

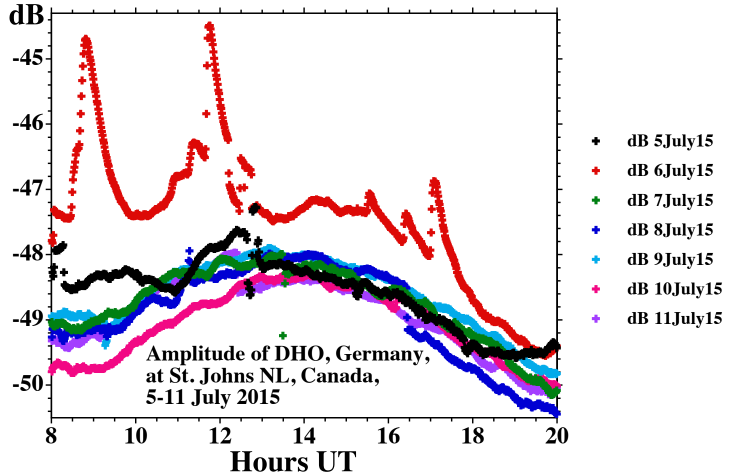
dB
-45
-46
-47
-48
-49
-50
8
10
12
14
16
18
20
Hours UT
Amplitude of DHO, Germany,
at St. Johns NL, Canada,
5-11 July 2015
dB 5July15
dB 6July15
dB 7July15
dB 8July15
dB 9July15
dB 10July15
dB 11July15

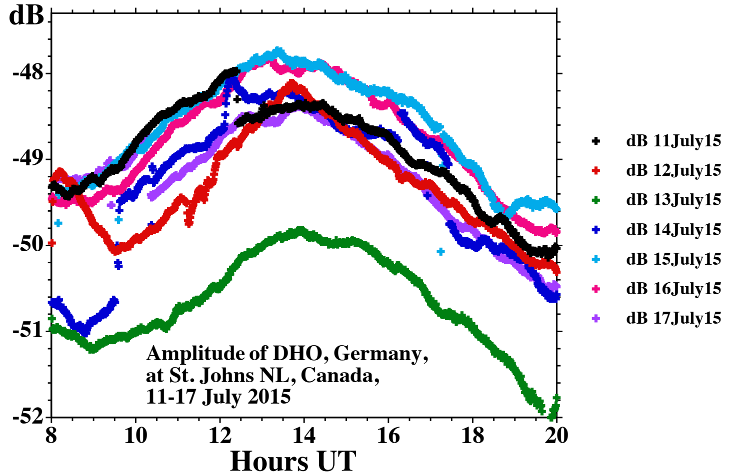
dB
-48
-49
-50
-51
-52
8
10
12
14
16
18
20
Hours UT
Amplitude of DHO, Germany,
at St. Johns NL, Canada,
11-17 July 2015
dB 11July15
dB 12July15
dB 13July15
dB 14July15
dB 15July15
dB 16July15
dB 17July15

Figure 3.

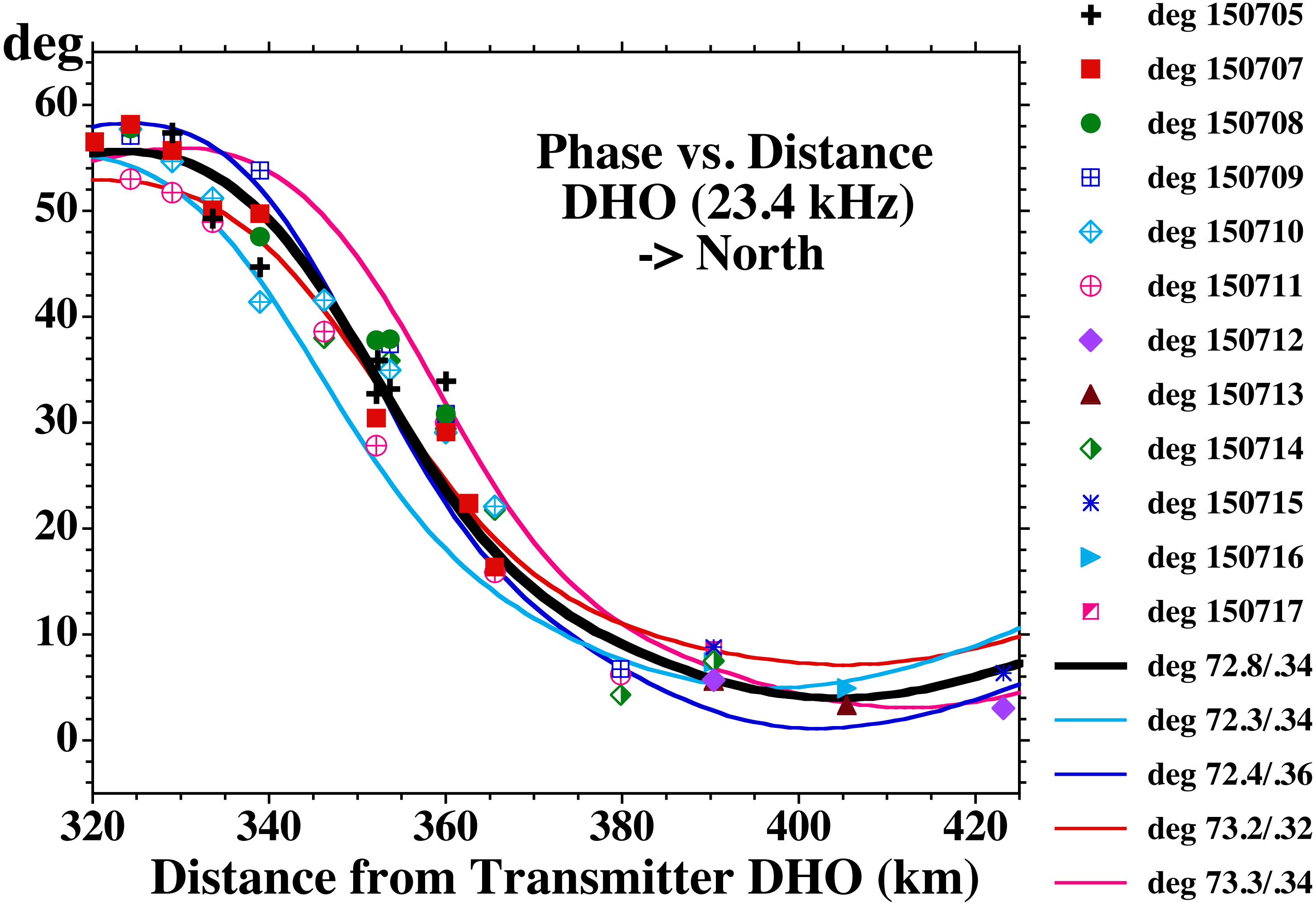
deg
Phase vs. Distance
DHO (23.4 kHz)
-> North
60
50
40
30
20
10
0
320
340
360
380
400
420
Distance from Transmitter DHO (km)
deg 150705
deg 150707
deg 150708
deg 150709
deg 150710
deg 150711
deg 150712
deg 150713
deg 150714
deg 150715
deg 150716
deg 150717
deg 72.8/.34
deg 72.3/.34
deg 72.4/.36
deg 73.2/.32
deg 73.3/.34

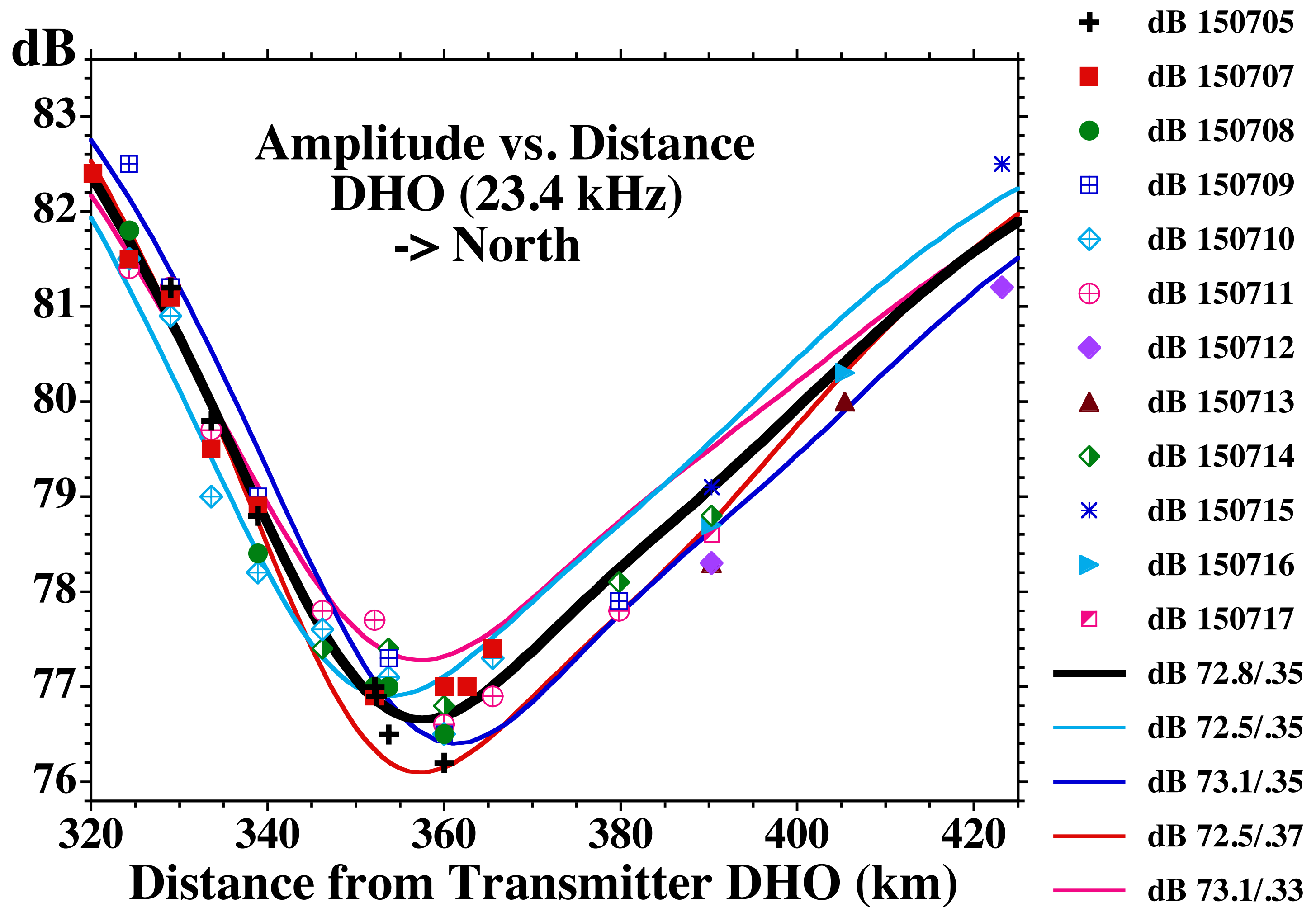
dB
Amplitude vs. Distance
DHO (23.4 kHz)
-> North
83
82
81
80
79
78
77
76
320
340
360
380
400
420
Distance from Transmitter DHO (km)
dB 150705
dB 150707
dB 150708
dB 150709
dB 150710
dB 150711
dB 150712
dB 150713
dB 150714
dB 150715
dB 150716
dB 150717
dB 72.8/.35
dB 72.5/.35
dB 73.1/.35
dB 72.5/.37
dB 73.1/.33

Figure 4.

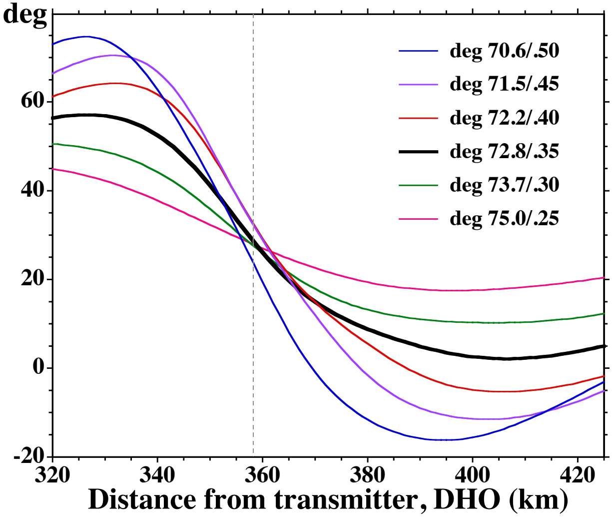
deg
60
40
20
0
-20
deg 70.6/.50
deg 71.5/.45
deg 72.2/.40
deg 72.8/.35
deg 73.7/.30
deg 75.0/.25
320
340
360
380
400
420
Distance from transmitter, DHO (km)

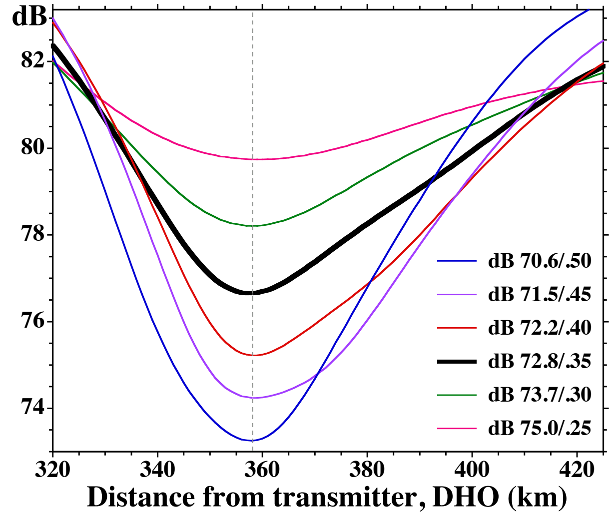
dB
82
80
78
76
74
dB 70.6/.50
dB 71.5/.45
dB 72.2/.40
dB 72.8/.35
dB 73.7/.30
dB 75.0/.25
320
340
360
380
400
420
Distance from transmitter, DHO (km)

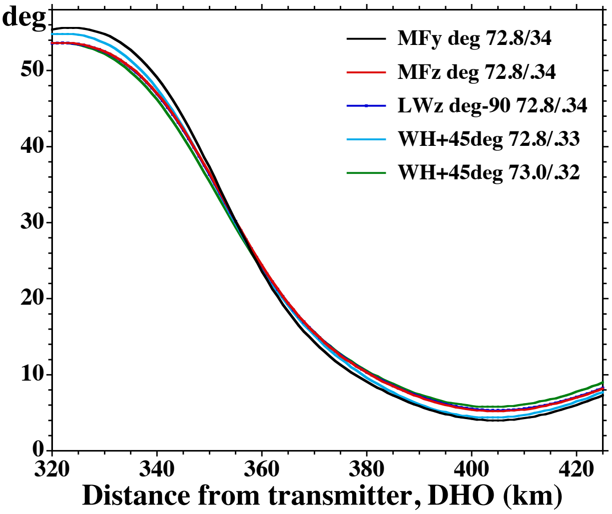
deg
50
40
30
20
10
0
MFy deg 72.8/34
MFz deg 72.8/34
LWz deg-90 72.8/.34
WH+45deg 72.8/.33
WH+45deg 73.0/.32
320
340
360
380
400
420
Distance from transmitter, DHO (km)

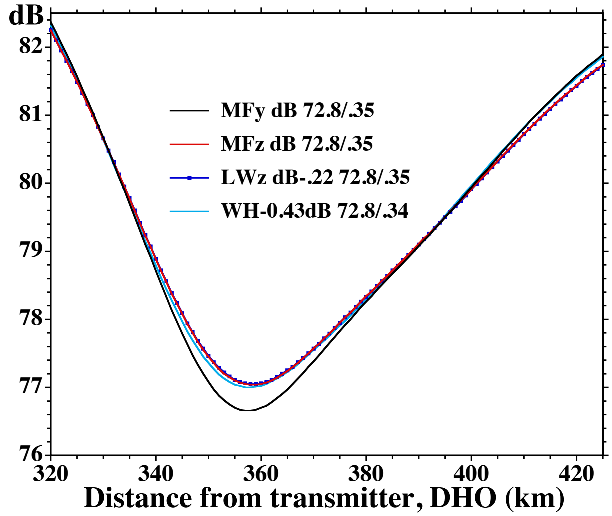
dB
82
81
80
79
78
77
76
MFy dB 72.8/.35
MFz dB 72.8/.35
LWz dB-.22 72.8/.35
WH-0.43dB 72.8/.34
320
340
360
380
400
420
Distance from transmitter, DHO (km)

Figure 5.

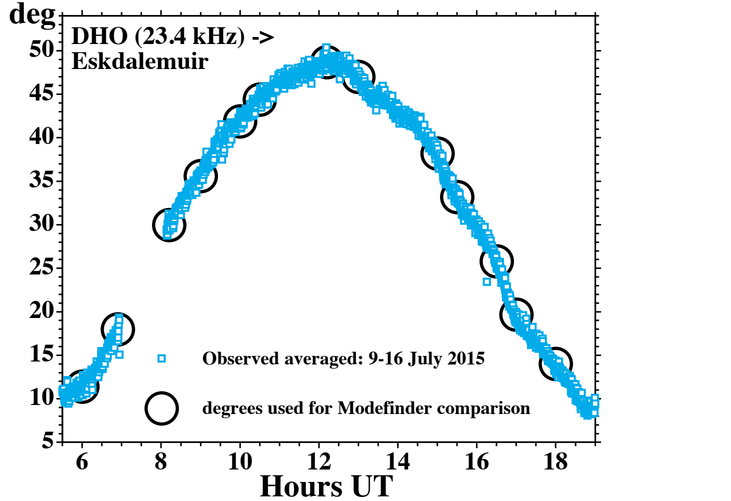
deg
DHO (23.4 kHz) ->
Eskdalemuir
Observed averaged: 9-16 July 2015
degrees used for Modefinder comparison
Hours UT

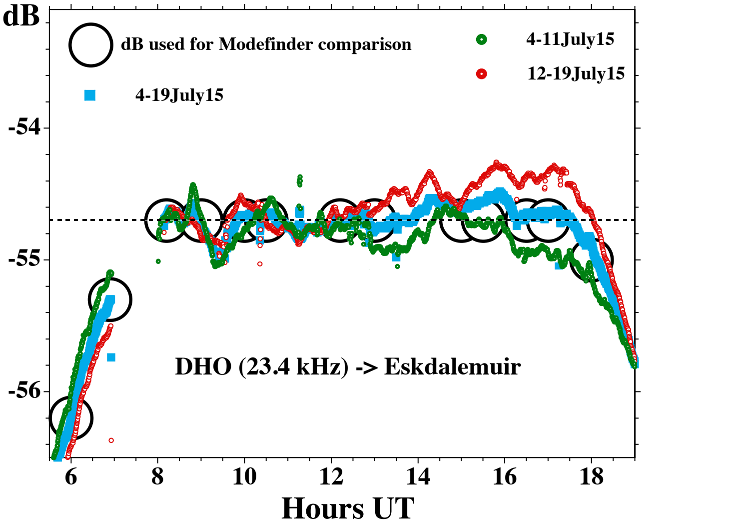
dB
dB used for Modefinder comparison
4-11July15
12-19July15
4-19July15
DHO (23.4 kHz) -> Eskdalemuir
Hours UT

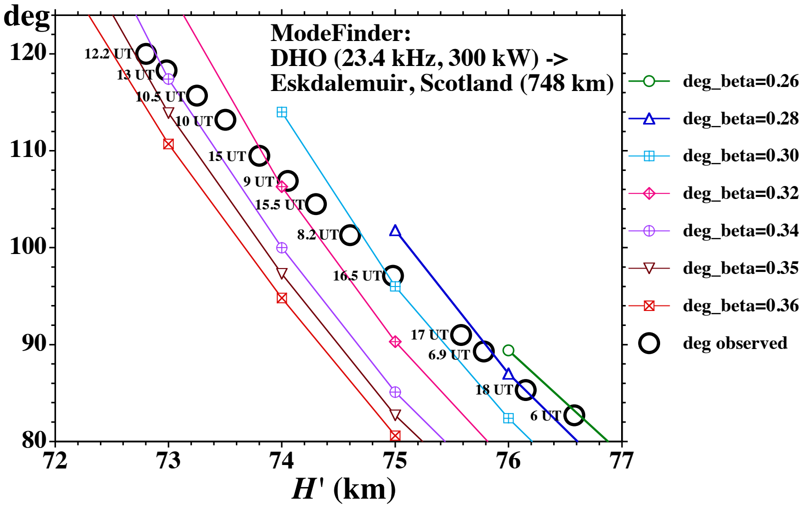
deg
ModeFinder:
DHO (23.4 kHz, 300 kW) ->
Eskdalemuir, Scotland (748 km)
12.2 UT
13 UT
10.5 UT
10 UT
15 UT
9 UT
15.5 UT
8.2 UT
16.5 UT
17 UT
6.9 UT
18 UT
6 UT
deg_beta=0.26
deg_beta=0.28
deg_beta=0.30
deg_beta=0.32
deg_beta=0.34
deg_beta=0.35
deg_beta=0.36
deg observed
H' (km)

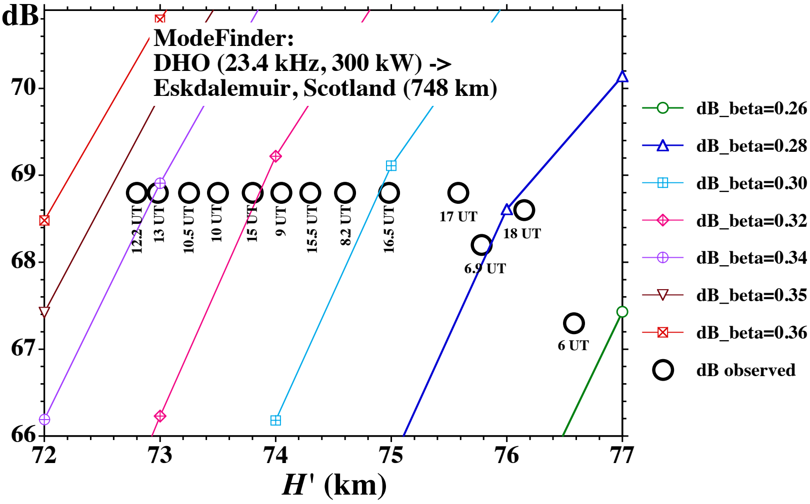
dB
ModeFinder:
DHO (23.4 kHz, 300 kW) ->
Eskdalemuir, Scotland (748 km)
12.2 UT
13 UT
10.5 UT
10 UT
15 UT
9 UT
15.5 UT
8.2 UT
16.5 UT
17 UT
18 UT
6.9 UT
6 UT
dB_beta=0.26
dB_beta=0.28
dB_beta=0.30
dB_beta=0.32
dB_beta=0.34
dB_beta=0.35
dB_beta=0.36
dB observed
H' (km)

Figure 6.

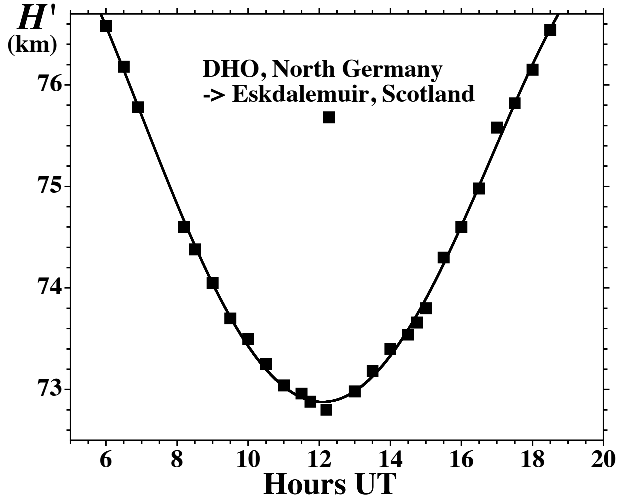
H' (km)
76
75
74
73
DHO, North Germany
-> Eskdalemuir, Scotland
6 8 10 12 14 16 18 20
Hours UT

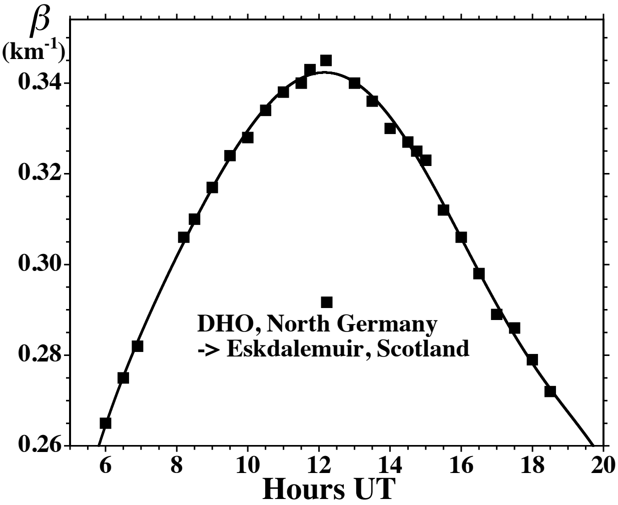
β (km-1)
0.34
0.32
0.30
0.28
0.26
DHO, North Germany
-> Eskdalemuir, Scotland
6 8 10 12 14 16 18 20
Hours UT

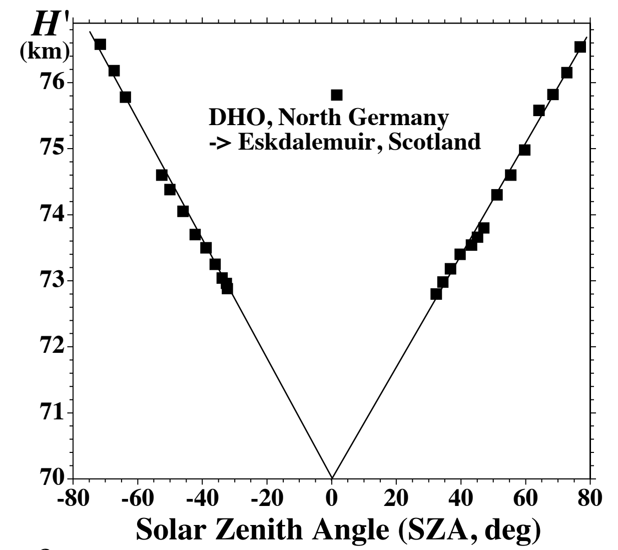
H' (km)
76
75
74
73
72
71
70
DHO, North Germany
-> Eskdalemuir, Scotland
-80 -60 -40 -20 0 20 40 60 80
Solar Zenith Angle (SZA, deg)

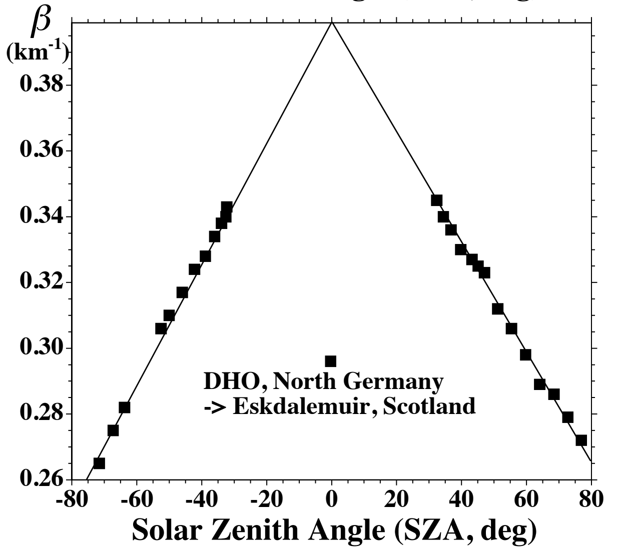
β (km-1)
0.38
0.36
0.34
0.32
0.30
0.28
0.26
DHO, North Germany
-> Eskdalemuir, Scotland
-80 -60 -40 -20 0 20 40 60 80
Solar Zenith Angle (SZA, deg)